Mutual synchronization of nanoconstriction-based spin Hall nano-oscillators through evanescent and propagating spin waves

T. Kendziorczyk* and T. Kuhn

Institut für Festkörpertheorie, Universität Münster, Wilhelm-Klemm-Straße 10, 48149 Münster, Germany

(Received 29 July 2015; revised manuscript received 21 March 2016; published 11 April 2016)

We perform a micromagnetic study of the synchronization dynamics in nanoconstriction-based spin Hall nano-oscillator (SHNO) arrays. The simulation reveals that efficient synchronization in this kind of system is possible, and indicates that the synchronization is mediated by a combination of linear coupling through the overlap of localized modes and parametric coupling through propagating spin waves which are excited by the second harmonic oscillation in the SHNOs. Due to the anisotropic spin wave dispersion in the studied system, the synchronization properties decisively depend on the geometrical alignment of the SHNO array with respect to the external field. We find that, by utilizing the directional spin wave emission and correspondingly optimizing the alignment of the SHNO array, the synchronization is enhanced with a significant increase of the phase-locking bandwidth.

DOI: 10.1103/PhysRevB.93.134413

I. INTRODUCTION

Since the first theoretical predictions of the spin-transfer torque (STT) [1,2], current-induced magnetization dynamics has been a very active research topic, leading to the development of nanoscale magnetic auto-oscillators—the so called spin-torque nano-oscillators (STNOs) [3–5]. STNOs are of high fundamental interest, because they form a testbed for different branches of physics, such as spin-dependent transport theory, magnonics, and nonlinear dynamics. Furthermore STNOs are promising for application as future GHz oscillators [6]. STNOs have some attractive advantages compared to conventional CMOS based oscillators, such as their nanoscale dimensions, a high frequency tunability, and ultrafast modulation [7]. However, they are also subject to several drawbacks, such as low output power and comparably large linewidths at roomtemperature. It is believed that these limitations can be overcome by implementing arrays of multiple synchronized STNOs [8–15]. Although much effort has been expended on this topic to date, a complete synchronization has been achieved only for a maximum number of five STNOs [16], mainly due to technological limitations which prevent a reliable fabrication of larger arrays [14].

Recently a new class of spintronic devices based on the spin Hall effect (SHE) [17,18] emerged. It has been demonstrated in several experiments that this effect can provide a sufficiently large STT to efficiently induce magnetization dynamics such as domain wall motion, magnetic switching, and the manipulation of magnetic damping [19–27]. Recently also autonomous oscillators similar to conventional STNOs have been found [28–31]. These oscillators are referred to as spin Hall nano-oscillators (SHNOs). SHNOs are based on a bilayer system consisting of a ferromagnet and an adjacent metal layer with strong spin orbit coupling. Here a perpendicular pure spin current is induced by the SHE in the metal by spin-dependent scattering of an in-plane electric charge current. Therefore a fully planar design with the same lateral geometry of both layers becomes possible [31]. Due to the reduced fabrication complexity, this kind of system could bring arrays of synchronized magnetic oscillators a step closer to the targeted application.

In this paper we provide a numerical analysis of the synchronization in a SHNO array by means of micromagnetic simulations. We find that, although the excited modes in the single SHNOs are localized, spin waves contribute to the synchronization. These spin waves are excited at the second harmonic frequency of the SHNO and mediate the synchronization by means of parametric excitation [32]. This is a mechanism which is different from previously studied mutually synchronized STNOs and also highly interesting from the general viewpoint of nonlinear physics, since here we have a simultaneous synchronization of oscillators by two modes with different frequencies and different localization behavior.

II. SYSTEM AND THEORETICAL FRAMEWORK

Figure 1(a) shows the studied SHNO array. The single SHNO geometry is chosen to match the experiment from Ref. [31]. The SHNOs consist of 150 nm wide nanoconstrictions in a Pt(8)/Py(5) (thickness in nm) bilayer system. Each constriction is defined through two cutoff wedges with a curvature radius of 50 nm and an opening angle of 11°. In the general case we consider an array of two SHNOs with relative lateral shifts Δx and Δy. The bilayer is traversed by an in-plane current with a total amplitude I_{SHNO}. An external magnetic bias field with the amplitude $H_0 = 450$ Oe is applied under an angle of $\alpha = 30^\circ$ with respect to the x axis.

We perform the numerical study with our finite differences time domain code [15], which solves the Landau-Lifshitz-Gilbert equation for the Py layer including the SHE induced torque term $\boldsymbol{\tau}_{\mathrm{SHE}} = \frac{\beta}{M_0^2}\boldsymbol{M} \times (\boldsymbol{M} \times [\boldsymbol{e}_z \times \boldsymbol{j}_{\mathrm{Pt}}])$ [19]. The prefactor $\beta = g\mu_{\mathrm{B}}\alpha_H/(2et_{\mathrm{Py}})$ contains the g factor, the electron-charge e, the layer thickness t_{Py}, and the spin Hall angle α_H. The electric current distribution and the Oersted fields are obtained by numerical solution of the electrostatic Poisson equation, together with Ohm's law for the two-layer system and employing Ampère's law [33].

As system parameters we use a saturation magnetization of $M_0 = 600$ kA/m, a Gilbert damping constant of $\alpha_G = 0.015$, an exchange stiffness of $A = 1.3 \times 10^{-11}$ J/m, and a spin Hall

*t.kend@uni-muenster.de

 ©2016 American Physical Society

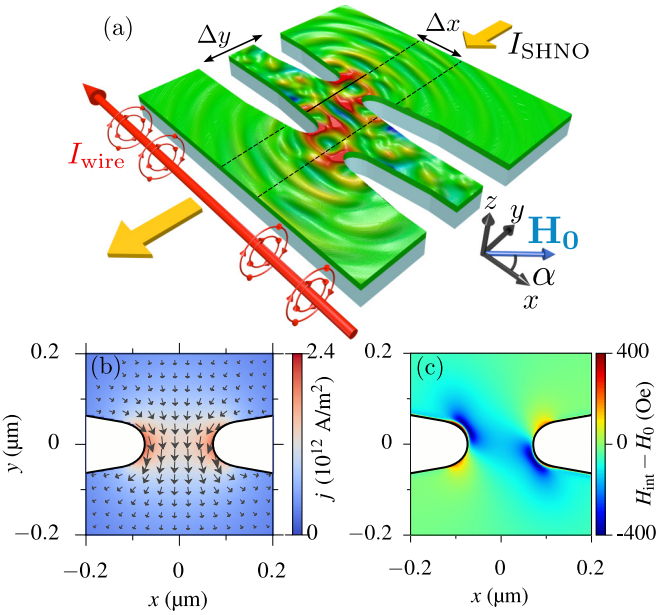

FIG. 1. (a) Schematic representation of the SHNO array. (b) Current density and (c) internal field in the Py layer for a single constriction and a total current of $I_{SHNO} = 2$ mA.

angle of $\alpha_H = 0.08$ [19]. The electric conductivities are set to $\sigma_{Py} = 3.07 \times 10^6$ S/m and $\sigma_{Pt} = 8.93 \times 10^6$ S/m [31].

III. SINGLE OSCILLATOR IN THE FREE-RUNNING REGIME

In the first part of our micromagnetic study we consider only one constriction defining a single free-running SHNO. We calculate the current distribution, the Oersted field, and the equilibrium orientation of the magnetization with the corresponding internal field. Figure 1(b) shows the current density distribution in the Pt layer for a single constriction. An identical distribution is obtained in the Py layer due to the same lateral geometry; however, more than 82% of the total current flows through the Pt layer. For a total current $I_{SHNO} = 2$ mA the maximal current density is 2.4×10^{12} A/m^2. The maxima are located close to the borders of the nano-constriction.

Figure 1(c) shows the internal field which is calculated within a micromagnetic simulation without the STT term, but including the Oersted fields. The internal field in the constriction is strongly reduced in an elliptical-shaped region with its long axis oriented perpendicular to the external field. It has two strong minima near the boundaries of the constriction.

We begin the analysis of the system dynamics with Fig. 2(a), which shows the power spectral density (PSD) calculated from the time trace of the spatially averaged dynamical magnetization in the center of the SHNO, after instantaneously applying the current I_{SHNO}. We find an oscillation with the frequency $f = 4.95$ GHz at the critical current $I_{C1} = 1.5$ mA. The frequency shows a nonlinear redshift with $df/dI = -80$ MHz/mA. In agreement with the experiment we observe a second critical current $I_{C2} = 4.5$ mA, where a second peak in the frequency spectrum appears and the oscillation becomes highly irregular with a strong linewidth broadening. Furthermore in the regime $I_{SHNO} < I_{C2}$ the PSD shows a significant spectral feature at the nonlinear second harmonic corresponding to the frequency $2f$. This oscillation is particularly pronounced for currents well above the critical current. The maximum of the ratio between the second- and first-order harmonic is larger than 30% and is reached at $I_{SHNO} = 3.5$ mA. We restrict our study in this paper to the single-mode regime $I_{C1} < I < I_{C2}$. In order to shine more light on the nature of the excited mode, we calculate

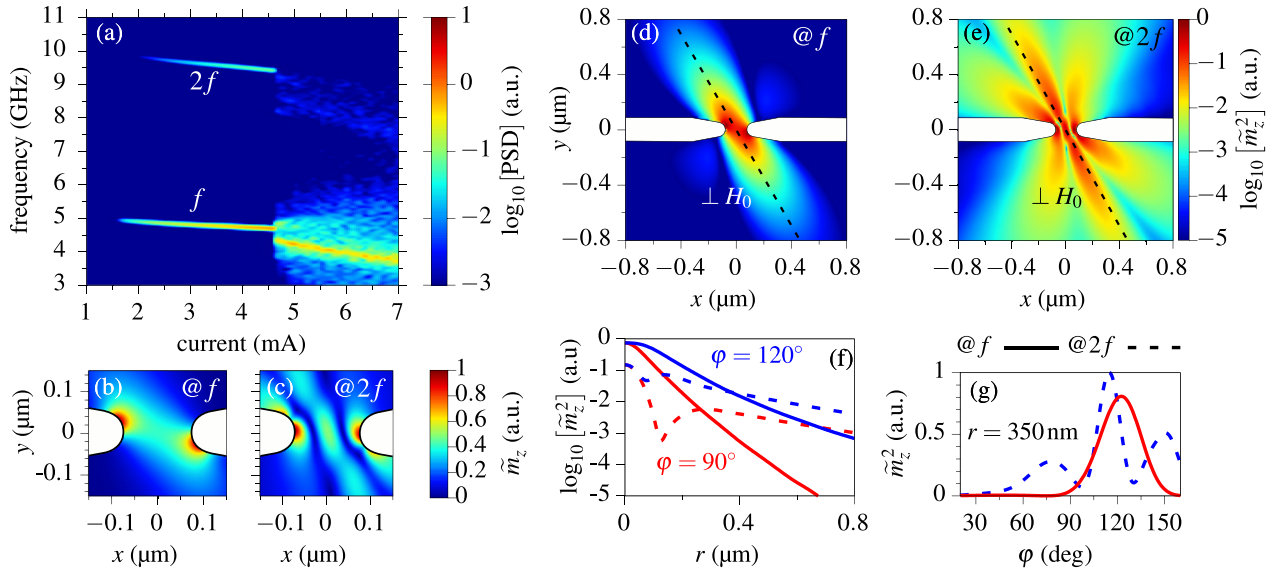

FIG. 2. (a) Power spectral density (PSD) calculated from the spatially averaged dynamic magnetization in a single SHNO. (b)–(f) Spatial amplitude distribution of the m_z component for $I_{SHNO} = 2$ mA at the fundamental frequency f and second harmonic $2f$. (b) and (c) Mode amplitude profiles in the constriction region on a linear color scaling. (d) and (e) Power distribution on a logarithmic color scaling for the whole surrounding film. The dashed line shows the direction perpendicular to the external field ($\perp H_0$). (f) Radial profiles in the direction with angles φ, which are defined with respect to the x axis. (g) Angular profiles for a constant distance $r = 350$ nm as a function of φ.

its spatial profile at the auto-oscillation frequency f for $I_{\mathrm{SHNO}} = 2$ mA. Figure 2(b) shows the amplitude distribution $\widetilde{m}_z(x,y,f)$ resulting from the temporal Fourier transform of the z component of the dynamical magnetization in a small region close to the constriction. Additionally we plot the spatial power distribution $\widetilde{m}_z^2$ for the whole layer in Fig. 2(d). We can observe a localized mode with a size (FWHM with respect to the power) of 240 nm perpendicular to the external field (dashed line) and 110 nm parallel to the external field. Therefore the mode has a strong elongation in the direction perpendicular to the external field, consistent with the experiment [31]. Furthermore the mode is much larger than the width of a typical self-localized bullet mode [34], whose size was determined in previous studies as about 80 nm [35]. By comparing the spatial amplitude distribution [Fig. 2(b)] with the internal field [Fig. 1(c)], we clearly identify that the shape of the mode is very similar to the profile of the internal field. The two maxima of the amplitude are exactly located in the regions with low internal fields. These results support the interpretation [31] that the studied SHNO is based on a localized mode in the effective static magnetic potential created by the inhomogeneous internal field rather than on a self-localized bullet mode, which can be observed in homogeneous ferromagnetic films.

In the following we analyze the oscillation at the second harmonic $2f$. Figure 2(c) shows the spatial amplitude of these dynamics in the region of the constriction. Similarly to the spatial profile of the first harmonic, the amplitude has two pronounced maxima close to the borders of the constriction. However, here we observe an additional maximum located in the center of the constriction. This can be explained by interference of spin waves which can be emitted due to the fact that the frequency $2f$ is well above the ferromagnetic resonance $f_{\mathrm{FMR}} = 5.31$ GHz, in contrast to the frequency f of the localized mode. By providing further analysis of the spatial distribution in a larger region outside the constriction [see Figs. 2(e)–2(g)], we can show that an efficient emission of spin waves is possible. We perform a fit of the spin wave intensity [36] to $\widetilde{m}_z^2 \propto \frac{1}{r} e^{-2r/\xi}$, where r is the distance from the center of the SHNO and ξ denotes the decay length of the spin wave amplitude. The fit is performed to a radial profile through the intensity emitted perpendicular to the external field which corresponds to an angle $\varphi = 120^\circ$ with respect to the x axis [see Fig. 2(f)]. This yields $\xi_{2f} = 930$ nm, which is more than twice the decay length of the evanescent wave with $\xi_f = 404$ nm. These values depend strongly on the emission direction, which can be seen in Fig. 2(g), where the angular profile of the spin wave intensity as a function of φ with a radius of $r = 350$ nm is plotted. The emitted spin waves have a strong directionality with emission perpendicular to the external field, which is an expected result considering the anisotropic dispersion in the studied in-plane magnetized system [36,37]. While the intensity of the evanescent spin waves has a single maximum for emission in the direction $\varphi = 120^\circ$, the main peak in the intensity for the spin waves $2f$ is shifted to smaller angles and there are several maxima and minima present. This is because the two observed maxima in the amplitude inside the constriction [see Fig. 2(c)] provide two separate coherent sources for spin waves which are well separated. Therefore the observed spatial profile of the emitted spin waves can be explained in terms of spin wave interference.

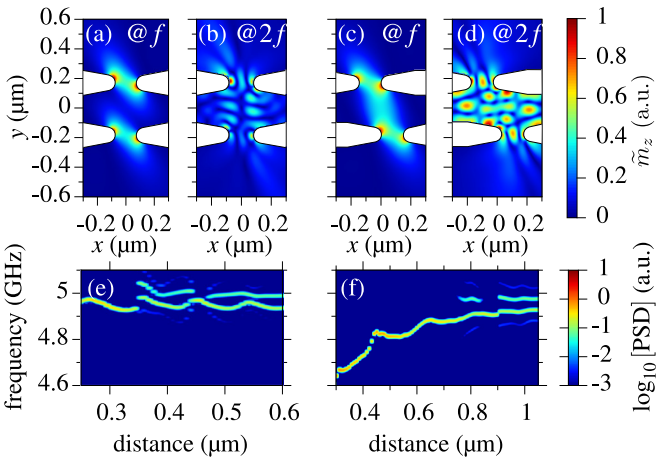

FIG. 3. (a)–(d) Spatial amplitude profile of m_z for two synchronized SHNOs with $I_{\mathrm{SHNO}} = 2.0$ mA for (a),(b) $\Delta x = 0$ nm and for (c),(d) $\Delta x = d_{H\perp}$. (e) and (f) Sum of the PSDs calculated from signals of two SHNOs for (e) $\Delta x = 0$ nm and (f) $\Delta x = d_{H\perp}$.

In order to obtain the wavelengths of the emitted spin waves, we furthermore analyze the spatial distribution of the phases of the emitted spin waves. The analysis yields values of $\lambda = 125$ nm for the emission parallel to the external field and $\lambda = 180$ nm for the emission perpendicular to the external field, which is in very good agreement with the spin wave dispersion [37] of an infinitely extended Py layer. This gives additional proof that the SHNO can indeed excite propagating spin waves at the frequency $2f$.

IV. SYNCHRONIZATION OF TWO OSCILLATORS

In the remainder of the paper we analyze the synchronization dynamics of an array with two SHNOs. We propose an array geometry which is designed to increase the mutual exchange of spin waves by utilizing the strongly directional emission of the spin waves perpendicular to the external field. Therefore, for two SHNOs with a distance of Δy in y direction, we compare two different structures: a conventional, aligned one ($\Delta x = 0$) and one which includes a shift of $\Delta x = d_{H\perp} = \Delta y \tan\alpha$ [see Fig. 1(a)]. In the latter case the direction perpendicular to the external field forms a direct connection line through the points in the center of the nanoconstrictions. The spin wave amplitudes for $I_{\mathrm{SHNO}} = 2$ mA and $\Delta y = 350$ nm are plotted in Figs. 3(a) and 3(b) for $\Delta x = 0$ nm and in Figs. 3(c) and 3(d) for $\Delta x = d_{H\perp} = 202$ nm. As expected from the single SHNO propagation properties [see Fig. 2(f)], in the case $\Delta x = d_{H\perp}$ we find a much larger amplitude of the evanescent spin wave and the interference pattern produced by the propagating spin waves in between both SHNOs. In order to investigate the influence of the achieved increased mutual spin wave emission, we study the synchronization dynamics as a function of $d = \sqrt{\Delta x^2 + \Delta y^2}$. The sum of the two PSDs calculated individually from the oscillation signal produced by both SHNOs is shown in Figs. 3(e) and 3(f). We have introduced a small mismatch

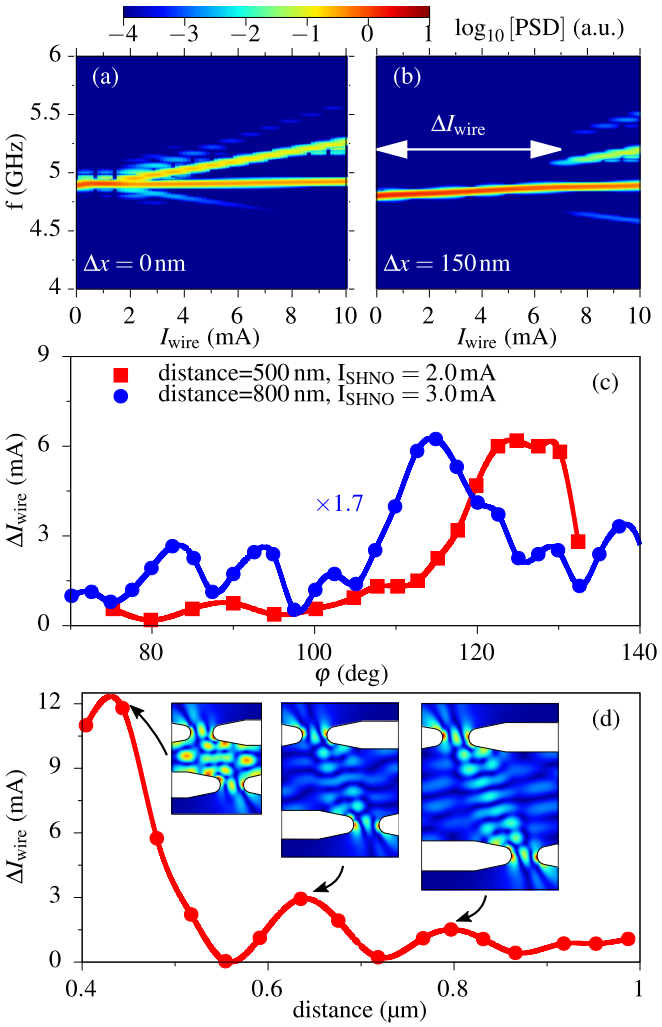

FIG. 4. (a) and (b) Sum of the PSDs calculated from the signals of two SHNOs under the influence of a nanowire with I_{wire} for (a) $\Delta x = 0$ nm and (b) $\Delta x = 150$ nm, $I_{\mathrm{SHNO}} = 2.0$ mA. (c) Size of the synchronization region ΔI_{wire} as a function of the angle φ for different values of I_{SHNO}. (d) ΔI_{wire} as a function of the SHNO distance for a fixed value $\varphi = 120°$, $I_{\mathrm{SHNO}} = 2.0$ mA. The insets show the spatial amplitude profile for the second harmonic $\widetilde{m}_z(2f)$. The lines are guides to the eye.

in the free-running frequencies by increasing the width of one of the constrictions to 170 nm. This ensures that we can clearly distinguish synchronized regions (single peak in the frequency spectrum) from unsynchronized regions (multiple peaks in the frequency spectrum). In the simple geometry [Fig. 3(e)] we find synchronization for distances below $d < 350$ nm and in a very small region close to $d = 450$ nm. In the case of the optimized geometry [Fig. 3(f)], synchronization is possible for much larger distances, up to $d = 750$ nm. Interestingly the frequency spectra reveal a pronounced periodic behavior with a periodicity corresponding to the wavelength of the spin waves emitted at the second harmonic, which will be analyzed in more detail below [see the discussion of Fig. 4(d)]. For larger distances the simulation results also show synchronized and unsynchronized regions alternately as a function of the distance. Both features are expected from the theory of mutual phase locking in auto-oscillators [10,38] and previous micromagnetic simulations [11,15] if the synchronization is mediated by propagating spin waves. Therefore the simulation of the SHNO array indicates that the spin waves emitted at the second harmonic contribute to the mutual synchronization. This can be explained by parametric coupling of the emitted spin waves by each SHNO with the auto-oscillation mode of the other SHNO respectively. Experimental proof for parametric synchronization of nanocontact STNOs has been provided already in Ref. [32]. However, in contrast to the present paper, the synchronization was achieved by excitation of the auto-oscillator with an external microwave signal with a frequency of twice the auto-oscillator frequency. Here this signal intrinsically appears as the nonlinear second harmonic of the oscillation from the SHNOs themselves and provides a channel for mutual synchronization via spin waves. The observed mutual parametric coupling is a distinct feature for the studied SHNO array, which is caused by the fact that here the fundamental mode is below the spin wave spectrum and has a strong attenuation. The second harmonic has still quite low relaxation frequencies and and has a large amplitude compared to the localized mode for reasonable distances. In contrast to this, in typical nanocontact STNOs the fundamental mode is already propagating—the so called Slonczewski mode [39,40]. These spin waves are exchange dominated and the second harmonic frequency is so high that due to the strong attenuation no significant contribution to the synchronization is expected.

The focus of the last part of the paper is to investigate the origin of the synchronization and to show which synchronization mechanisms are particularly important based on the choice of the system parameters. This can be achieved by analyzing the phase-locking bandwidth for different conditions, which favor either linear synchronization or parametric synchronization mediated by spin waves. The phase-locking bandwidth is defined as the maximum frequency detuning for which synchronization is possible. In contrast to systems based on nanocontact STNOs with independent bias currents, here it is not directly possible to change the frequency detuning. We solve this problem in the simulation by introducing an additional external magnetic field with a spatial gradient which mainly influences one of the SHNOs. This could be realized for example by the Oersted field produced by a nanowire, which is sketched in Fig. 1(a). Figures 4(a) and 4(b) show that the detuning can be controlled by the current I_{wire} through the nanowire. While the frequency of the SHNO close to the wire experiences a linear shift with about 42 MHz/mA, the frequency of the second SHNO is barely affected. Therefore we can identify the phase-locking region ΔI_{wire}, which is approximately proportional to the phase-locking bandwidth.

In Fig. 4(c) we examine the value ΔI_{wire} as a function of φ, which is the angle between the center-to-center connection line between the SHNOs with the x axis. We perform these calculations for two different parameter sets: (i) the squares show the simulation results for a distance of 500 nm with a current $I_{\mathrm{SHNO}} = 2.0$ mA and (ii) the points show the data for 800 nm with $I_{\mathrm{SHNO}} = 3.0$ mA. These parameters are chosen to prefer the linear synchronization by the overlap of the localized modes in case (i) and the spin wave mediated parametric synchronization in case (ii). This is because the influence of the parametric coupling increases for larger distances due to

the larger decay length $\xi_{2f} > \xi_f$ [see Fig. 2(e)]. Furthermore the parametric coupling becomes more important for larger current densities because the ratio between the power of the evanescent waves and propagating waves increases in this case [see Fig. 2(a)]. For better visibility the data for the larger distance (ii) have been multiplied by a factor 1.7 to compensate for the reduced synchronization bandwidth at the maximum, which is simply related to the spatial attenuation of both the localized and propagating modes. The data for parameter set (i) shows a pronounced maximum at an angle of $\varphi = 125^\circ$, which is close to the expected value of $\varphi = 120^\circ$, corresponding to $\Delta x = d_{H\perp}$ (alignment of the center-to-center connection line between the SHNOs perpendicular to the external field). The value for the phase locking-bandwidth at the conventional, aligned geometry with $\varphi = 90^\circ$ is reduced by a factor of 8 in comparison to the main maximum. In contrast to these results, the phase-locking bandwidth as a function of φ for the parameter set (ii) has multiple pronounced maxima at different values of φ. This can be explained by the fact that the propagating spin waves, which are generated by two sources at each constriction, can interfere. Therefore the results are reminiscent of the angular behavior obtained for a single SHNO [see Fig. 2(g)], which is characterized by one maximum for the localized mode and multiple maxima for the propagating modes. However, in the case of two SHNOs additional quantization effects can occur due to the finite extension of the permalloy film between the wedges defining the top and bottom constrictions. Therefore more complicated interference patterns are possible for the propagating spin waves [see Figs. 3(b) and 3(d)]. These observations are consistent with the increased number of side maxima in the phase-locking bandwidth as a function of φ.

The same method for obtaining the phase-locking bandwidth can be used to obtain the latter as a function of the SHNO distance. Figure 4(d) shows periodic features in the phase-locking bandwidth. To understand the reason for this periodicity in more detail, we show the spatial amplitude profile for the second harmonic $\tilde{m}_z(2f)$ in the insets of Fig. 4(d). These spatial profiles are calculated for SHNO distances corresponding to the values where we obtain maxima in the phase-locking bandwidth (see the arrows in the insets). For all distances we can see an interference pattern created by the spin waves emitted at the second harmonic. Comparing the number of maxima in the interference pattern for the chosen distances we obtain three, five, and seven maxima between the SHNOs. Therefore the difference in the distance between two maxima in the phase-locking bandwidth corresponds to one additional wavelength, which is again evidence for the parametric synchronization mediated by the spin waves at the second harmonic.

The obtained periodic behavior of the phase-locking bandwidth can explain the alternate appearance of synchronized and unsynchronized regions as a function of the distance in Figs. 3(e) and 3(f), because it shows that the phase-locking bandwidth is a nonmonotonic function, which in combination with a constant detuning between the SHNOs leads to the observed features. Furthermore this emphasizes the importance of taking into account the second harmonic spin waves in the design of an SHNO array, because for certain geometries the bandwidth can be significantly reduced.

V. CONCLUSION

In conclusion, we have performed a micromagnetic study of the synchronization in SHNO arrays. We found that, in contrast to previously studied nanocontact STNOs, the synchronization is composed of two mechanisms: linear synchronization through the overlap of the localized modes and parametric synchronization mediated by propagating spin waves which are excited by the nonlinear second harmonic of the SHNOs. The synchronization mechanism based on propagating spin waves can be favored in two ways. One of these ways is based on the geometry of the array. By choosing larger distances between the SHNOs, the influence of the localized modes is reduced due to their strong attenuation compared to the propagating spin waves. The second way is to operate the SHNOs at larger current densities. In this case the ratio between the amplitude of the second harmonic and the fundamental mode can be increased.

Furthermore our study revealed that it is important to take into account the directionality of the spin wave emission in the design of the SHNO array geometry. By proposing a geometry which maximizes the overlap of the spin wave modes, we show that the synchronization bandwidth can be substantially improved. This result applies for both synchronization mediated by the propagating mode and the localized one.

Our simulations therefore provide multiple general predictions for the operation of synchronized SHNOs which should be carefully considered in the design of future devices based on SHNO arrays.

ACKNOWLEDGMENT

The authors are grateful to S. O. Demokritov and V. E. Demidov for fruitful discussions.

[1] J. C. Slonczewski, J. Magn. Magn. Mater. **159**, L1 (1996).
[2] L. Berger, Phys. Rev. B **54**, 9353 (1996).
[3] M. Tsoi, A.-G.-M. Jansen, J. Bass, W.-C. Chiang, M. Seck, V. Tsoi, and P. Wyder, Phys. Rev. Lett. **80**, 4281 (1998).
[4] S.-I. Kiselev, J.-C. Sankey, I.-N. Krivorotov, N.-C. Emley, M. Rinkoski, C. Perez, R.-A. Buhrman, and D.-C. Ralph, Phys. Rev. Lett. **93**, 036601 (2004).
[5] W.-H. Rippard, M.-R. Pufall, S. Kaka, S.-E. Russek, and T.-J. Silva, Phys. Rev. Lett. **92**, 027201 (2004).
[6] P. Villard, U. Ebels, D. Houssameddine, J. Katine, D. Mauri, B. Delaet, P. Vincent, M.-C. Cyrille, B. Viala, J.-P. Michel *et al.*, IEEE J. Solid-State Circuits **45**, 214 (2010).
[7] R. K. Dumas, S. R. Sani, S. M. Mohseni, E. Iacocca, Y. Pogoryelov, P. K. Muduli, S. Chung, P. Dürrenfeld, and J. Åkerman, IEEE Trans. Magn. **50**, 4100107 (2014).
[8] S. Kaka, M. R. Pufall, W. H. Rippard, T. J. Silva, S. E. Russek, and J. A. Katine, Nature (London) **437**, 389 (2005).

[9] F.-B. Mancoff, N.-D. Rizzo, B.-N. Engel, and S. Tehrani, Nature (London) **437**, 393 (2005).
[10] A.-N. Slavin and V.-S. Tiberkevich, Phys. Rev. B **74**, 104401 (2006).
[11] X. Chen and R.-H. Victora, Phys. Rev. B **79**, 180402 (2009).
[12] D.-V. Berkov, Phys. Rev. B **87**, 014406 (2013).
[13] V. Puliafito, G. Consolo, L. Lopez-Diaz, and B. Azzerboni, Physica B **435**, 44 (2014).
[14] S. Sani, J. Persson, S. M. Mohseni, Y. Pogoryelov, P. K. Muduli, A. Eklund, G. Malm, M. Käll, A. Dmitriev, and J. Åkerman, Nat. Commun. **4**, 2731 (2013).
[15] T. Kendziorczyk, S. O. Demokritov, and T. Kuhn, Phys. Rev. B **90**, 054414 (2014).
[16] A. Houshang, E. Iacocca, P. Dürrenfeld, S. Sani, J. Åkerman, and R. Dumas, Nat. Nanotechnol. **11**, 280 (2016).
[17] M. I. D'yakonov and V. I. Perel, ZhETF Pis. Red. **13**, 657 (1971) [Sov. Phys. JETP **13**, 467 (1971)].
[18] J.-E. Hirsch, Phys. Rev. Lett. **83**, 1834 (1999).
[19] K. Ando, S. Takahashi, K. Harii, K. Sasage, J. Ieda, S. Maekawa, and E. Saitoh, Phys. Rev. Lett. **101**, 036601 (2008).
[20] L. Liu, T. Moriyama, D.-C. Ralph, and R.-A. Buhrman, Phys. Rev. Lett. **106**, 036601 (2011).
[21] I. M. Miron, K. Garello, G. Gaudin, P.-J. Zermatten, M. V. Costache, S. Auffret, S. Bandiera, B. Rodmacq, A. Schuhl, and P. Gambardella, Nature (London) **476**, 189 (2011).
[22] V. E. Demidov, S. Urazhdin, E.-R.-J. Edwards, M.-D. Stiles, R.-D. McMichael, and S.-O. Demokritov, Phys. Rev. Lett. **107**, 107204 (2011).
[23] L. Liu, O.-J. Lee, T.-J. Gudmundsen, D.-C. Ralph, and R.-A. Buhrman, Phys. Rev. Lett. **109**, 096602 (2012).
[24] L. Liu, C.-F. Pai, Y. Li, H. Tseng, D. Ralph, and R. Buhrman, Science **336**, 555 (2012).
[25] S. Emori, U. Bauer, S.-M. Ahn, E. Martinez, and G. S. Beach, Nat. Mater. **12**, 611 (2013).
[26] K.-S. Ryu, L. Thomas, S.-H. Yang, and S. Parkin, Nat. Nanotechnol. **8**, 527 (2013).
[27] P. Haazen, E. Murè, J. Franken, R. Lavrijsen, H. Swagten, and B. Koopmans, Nat. Mater. **12**, 299 (2013).
[28] V. E. Demidov, S. Urazhdin, H. Ulrichs, V. Tiberkevich, A. Slavin, D. Baither, G. Schmitz, and S. O. Demokritov, Nat. Mater. **11**, 1028 (2012).
[29] L. Liu, C.-F. Pai, D.-C. Ralph, and R.-A. Buhrman, Phys. Rev. Lett. **109**, 186602 (2012).
[30] R.-H. Liu, W.-L. Lim, and S. Urazhdin, Phys. Rev. Lett. **110**, 147601 (2013).
[31] V. E. Demidov, S. Urazhdin, A. Zholud, A. V. Sadovnikov, and S. O. Demokritov, Appl. Phys. Lett. **105**, 172410 (2014).
[32] S. Urazhdin, V. Tiberkevich, and A. Slavin, Phys. Rev. Lett. **105**, 237204 (2010).
[33] A. J. Newell, W. Williams, and D. J. Dunlop, J. Geophys. Res. **98**, 9551 (1993).
[34] A. Slavin and V. Tiberkevich, Phys. Rev. Lett. **95**, 237201 (2005).
[35] H. Ulrichs, V. E. Demidov, and S. O. Demokritov, Appl. Phys. Lett. **104**, 042407 (2014).
[36] V. E. Demidov, S. Urazhdin, and S. O. Demokritov, Nat. Mater. **9**, 984 (2010).
[37] B.-A. Kalinikos and A.-N. Slavin, J. Phys. C **19**, 7013 (1986).
[38] A. Slavin and V. Tiberkevich, IEEE Trans. Magn. **45**, 1875 (2009).
[39] J.-C. Slonczewski, J. Magn. Magn. Mater. **195**, L261 (1999).
[40] M. Madami, S. Bonetti, G. Consolo, S. Tacchi, G. Carlotti, G. Gubbiotti, F.-B. Mancoff, M. A. Yar, and J. Åkerman, Nat. Nanotechnol. **6**, 635 (2011).